Microresistivity and ultrasonic imagers: tool operations and processing principles with reference to commonly encountered image artefacts

PHILIP S. CHEUNG

Schlumberger Ribaud Product Center, 26 Rue de la Cavée, B.P. 202, 92142 Clamart, France

Abstract: Borehole images obtained from microresistivity and ultrasonic imager tools form an important source of geological information. The interpretation of these images is often hampered by the presence of artefacts, arising from peculiarities of the logging tools, and/or unexpected borehole conditions. In this paper, the operations of microresistivity and ultrasonic imager tools are reviewed, with a special emphasis on the tool features and borehole conditions that may give rise to artefacts in the resultant borehole images. The origin and characteristics of some commonly encountered artefacts are discussed, pointing out how they can be identified. Processing methods that may help to remove or reduce the effects of the artefacts are described. This information should help an interpreter to initially better understand the origin and significance of commonly encountered artefacts in terms of tool response, and secondly ensure that undesirable effects of such artefacts are minimised by using available data processing methods.

The author was invited to write this article to complement the paper by Lofts & Bourke (1999) *this volume*, titled 'The recognition of artefacts from acoustic and resisitivity borehole imaging devices'. As there was little time to gather publishable examples, permission was kindly given to use the examples presented by Lofts & Bourke. These examples from Lofts & Bourke will be referred to in short, for example, L&B 'Mud Smear', where the description in quotes is the label used by Lofts & Bourke in their paper.

The purpose of this paper is to summarize the information concerning the operation and data processing of microresistivity and ultrasonic imaging tools which is essential to the correct interpretation of the borehole images. In particular, it is intended to help an interpreter to initially better understand the origin and significance of commonly encountered artefacts in terms of tool response, and secondly ensure that undesirable effects of such artefacts are minimized by using available data processing methods. The following approach will be adopted in the paper. For each of the two types of imaging tools, the tool operations and sensor response will be outlined. Special features that may lead to artefacts are then discussed. The discussion will include pointers as to how artefacts may be recognized, and if processing methods are available, their theory and limitations. The physical basis for the appearance of various artefacts will be described in some detail, to enable an interpreter to assess their significance. In contrast, the various processing methods are only briefly mentioned, since details of algorithms would be beyond the scope of this article. Finally, the two tool types are discussed together in a summary section.

Microresistivity imagers

Tool operation

The following is a brief and general description of the operations of microresistivity imaging tools. Details of the actual tools available today are given by Ekstrom *et al.* (1987), Safinya *et al.* (1991), Seiler *et al.* (1994) and Lacazette (1996). In the complex logging environment, an understanding of the tool response can usually be achieved only by comparing logged data, cores and results from mathematical modelling. Trouiller *et al.* (1989) and Williams *et al.* (1997) provide further details of this process.

Microresistivity imagers are equipped with a number of pads with conducting surfaces, on which arrays of button electrodes are placed. When logging, the pads are pressed against the borehole wall and a voltage is applied between the lower section of the sonde, this includes the pads, and its upper section, which is separated from the lower section by an insulating section (Fig. 1). In consequence, currents will flow from the lower to the upper section of the sonde. Some currents will flow directly up the borehole

From: LOVELL, M. A., WILLIAMSON, G. & HARVEY, P. K. (eds) 1999. Borehole Imaging: applications and case histories. Geological Society, London, Special Publications, **159**, 45–57. 1-86239-043-6/99/$15.00.

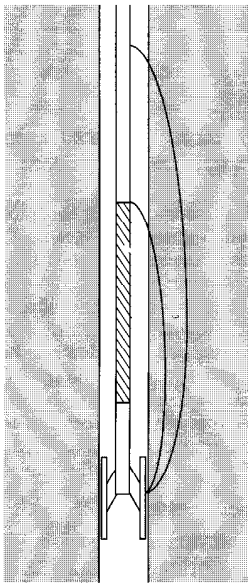

Fig. 1. Schematic showing a microresistivity tool and the path of the current emerging from a tool button.

through the mud. Currents emerging from the buttons will be focused by the conducting pad face into the formation, before returning eventually to the upper section of the sonde. The button currents are modulated by the conductivity of the formation directly in front of them, thereby allowing a qualitative conductivity image of the borehole wall to be constructed.

Figure 2 shows the button array typical of microresistivity tools currently in use. While the number of buttons may vary, their diameter is of the order of 5 mm, and they are usually arranged in two rows with a lateral offset to obtain a lateral sampling of half the button diameter, thus avoiding aliasing. The buttons on each pad image a strip of the borehole wall of fixed width. Different tools carry a different number of pads, on a different number of arms to provide different degrees of lateral coverage. In all cases, percentage cover of the borehole wall decreases as hole size increases.

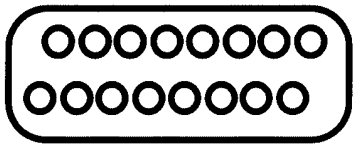

Fig. 2. Typical button arrangement on the pad of a microresistivity tool. Note that the image is formed by interlacing data from two rows of buttons which are offset in depth.

In order that the pads pack into a compact space when the tool is closed, the pads from most tools are located at different depths. For four-arm tools carrying two pads per arm, the second pad (referred to as a flap) is attached alongside and below the first pad, fixed directly on the arm. For six-arm tools, the odd and even numbered pads are displaced in depth. This depth offset of the pads, and the offset of the buttons on each pad, imply that the data acquired must be correctly aligned in depth to produce a correct image. Unless corrected, irregular tool speed during logging will give rise to certain artefacts in the image, this is discussed in more detail later.

Button sensor response

Since the pad face is a conductor forming an equipotential surface, the currents leaving it travel initially in the direction normal to the pad. In particular, the current flowing out of a button will be focused initially into a cylinder with a cross-sectional area equal to the button area. Almost immediately, the current diverges as the focusing influence of the pad face diminishes. Since the return electrode is effectively the entire upper section of the sonde, the current diffuses into a vast volume before entering the return electrode. This is shown schematically in Fig. 1.

The magnitude of the button current is equal to the applied voltage divided by the resistance of the current path. This resistance can be thought of qualitatively as consisting of two resistances in series. The first corresponds to the small volume facing the button where the current is focused, and the second, to the volume where the current is diffused. In each case:

$$\text{resistance} = \text{formation resistivity} \times (\text{path length}/\text{path cross-sectional area})$$

where the formation resistivity is some weighted average value for the volume concerned. The two resistances are in general comparable in magnitude: the path length and cross-sectional area being both small for the focused path, and large for the diffused path. By contrast, the focused resistance, pertaining to small volume, gives a high resolution measure of the formation resistivity, while the diffused resistance is a low resolution measure.

The button current as a function of depth will therefore consist of two distinct components: a high resolution component corresponding to the focused volume, with a resolution as high as the button size (5 mm); and a low resolution background corresponding to the diffused volume with a resolution as low as the sonde length

(≈10 m). On an image, one observes essentially the variations of high resolution component.

The button current is a qualitative conductivity measurement. While the concept of the focused and diffused components is useful in helping to understand the response of the tool, it is in practice difficult to separate the two components to give a quantitative conductivity.

Depth of investigation. When discussing the depth of investigation of a microresistivity device, it is clear that one refers to the high resolution component, since the information conveyed in the image is contained essentially in this component. From the above discussion, we expect the high resolution component to have a shallow depth of investigation. Indeed, if the depth of investigation were much deeper than one or two centimetres, the image will be a juxtaposition of features at different radial depths, which is not commonly observed.

Williams *et al.* (1997) investigated in detail the button response with respect to small inhomogeneities by mathematical modelling. Leaving aside subtle differences between the response to small conductive and resistive objects placed at different distances from the borehole wall, they arrive at a depth of investigation of 1–2 cm. Bourke *et al.*(1989) quoted a value of ≈2.5 cm. The electrical penetration parameter used to correct dips measured by microresistivity devices is another measure of depth of investigation. Using modelling results as well as the comparisons of dip values obtained from logs (dipmeter and image data) and core measurements, values between 1–2 cm are normally used. This evidence points to a very shallow depth of investigation.

A special circumstance should be noted concerning thin conductive beds or conductive fractures, sandwiched between two resistive layers. In such cases the depth of investigation is increased. An explanation for this phenomenon is given in the section *Distortions by Strong Contrast*. When computing dips for conductive features (for example, when the resistivity contrast between adjacent beds exceeds a factor of 10), it will be necessary to take into account a larger than normal electrical penetration. In theory, if rough values of the resistivity contrast and dip magnitude are known, then it is possible to compute a suitable electrical penetration parameter. In practice, this approach is not always feasible. It would be safer in such cases to compare dips from microresistivity devices with cores or other measurements. Hansen & Parkinson (1999) report a depth of investigation of 5–7 cm in a study comparing images from microresistivity and ultrasonic devices.

Trouiller *et al.* (1989) mention that in thick homogeneous or finely laminated beds, the depth of investigation of a button is similar to that of a shallow laterolog, which is roughly 25 cm. This comment has caused some confusion in the past. In fact, it applies only to the low resolution component, or the background value of the image (Trouiller, pers. comm. 1989). This does not mean that small inhomogeneities more than about 2 cm from the borehole wall would be observable.

Resolution. When the pad makes direct contact with a formation with no strong resistivity contrasts (e.g. <10), the theoretical resolution of the button approaches the value of its diameter (5 mm). In practice, the resolution can be much poorer (≈1 cm). Apart from errors arising from acquisition, such as irregular tool speed, there are two other factors which affect resolution: distortion by strong contrast and standoff. These will be discussed later under the heading, '*Special features related to artefacts*'.

Response to fractures. Luthi & Souhaité (1990) have shown by simulation that there will be an increase of button current in the neighbourhood of a fracture filled with conductive fluid. More precisely, the integral of the increase in the button current across the fracture trace is proportional to the product of the fracture aperture and the conductivity of the fluid in the fracture. By contrast, the apparent width of a fracture is unrelated to its aperture. In the majority of cases, the apparent width would be of the order of the button resolution of ≈5 mm, while the aperture would rarely exceed this value.

Given the conductivities of the fluid and the surrounding rock, an effective aperture can be obtained from the microresistivity button current response. Provided there is a strong resistivity contrast between the fluid in the fracture and the surrounding rock, apertures down to 10 μm are quantifiable. This technique has been applied to logged data by Hornby *et al.* (1992).

The work of Luthi & Souhaité (1990) is limited to fracture dip angles below 40°. To apply the technique successfully, the interpreter must take care to select only open fractures (since the method will give an 'answer' for any conductive feature), and have an accurate knowledge of the conductivity of the in-filling fluid.

Special features related to artefacts

Tool speed variations. Most logging systems record data as a function of cable depth, i.e. a

frame of data is recorded each time the cable at wellhead is detected as having moved a fixed distance, this being ≈ 2.5 mm in the case of a microresistivity imaging tool. Since the cable is elastic, the movement of the cable at wellhead does not always correspond to the movement of the tool at a given instant of time. A log will be stretched/compressed locally when the tool speed is below/above the cable speed i.e. the data attributed to a given depth interval is in fact acquired over a smaller/larger distance. In the extreme case, the tool may become stuck i.e. the tool remains stationary while the cable continues to wind in. In this case, the same data will be recorded over several cable depths. This results in pronounced stretching of the image (L&B 'Tool Speed Irregularities – Stuck zones'). As the tool eventually frees itself, it accelerates due to the buildup of tension in the cable, causing the image to be severely compressed. When a tool is conveyed by tubing or casing, stick-and-slip can also occur. Since these are less elastic than a cable, the motion is more jerky, in a series of short stick-and-slips. All logs and images suffer from alternating compression and stretching to some degree unless corrected. Quite naturally, the effects on images are particularly dramatic. The distortions would lead to errors in bed thickness and dip estimation.

Stretching and compressing have another effect unique to microresistivity imagers. Since the sensors are not at the same depth, they will pass a given depth at different times. At these different times, the tool speed will not in general be the same. Thus at a given depth interval, the degree of stretching or compression will be different for the sensors offset in depth. The resultant image obtained by assembling the data from the different sensors will therefore contain depth mismatches. When each pad contains two rows of buttons interlaced laterally but separated in depth, the depth mismatch of the two rows will give rise to saw-teeth distortions across the pad image (L&B 'Tool speed irregularities – sticky zones'). Similarly, when adjacent pads suffer from depth mismatch, geological features will become discontinuous going from one pad to the next (L&B 'Pad-flap or button offsets').

Correction for tool speed is done using an accelerometer located along the tool axis. Chan (1984) describes how the acceleration can be integrated, using the cable depth as a constraint by means of a Kalman filter, to give estimates of the tool velocity and depth. This is an important advance on earlier efforts, because the Kalman filter allowed the constraint to be applied in a continuous fashion. Chapellat *et al.* (1996) have proposed a second method which uses the correlations between button values measured on the two rows to estimate the degree of compression and stretching, and hence the tool velocity relative to cable speed. This latter method is usually applied after the accelerometer based method although it can also be used on its own, as when the accelerometer malfunctions. It is most obviously effective in correcting 'saw-teeth' but leads to significant improvements even when 'saw-teeth' are not apparent.

With these methods, and their refinements over the years, speed correction problems have become less frequent. There are nevertheless cases, especially in highly deviated wells, when speed correction is unsatisfactory. It is worth pointing out that speed correction relies on measurements which themselves suffer from error. For example, the accelerometer measurement has at least three limitations:

- imperfect separation of tool acceleration and the gravitational acceleration component which are measured simultaneously by the accelerometer
- precision and frequency (transient) response of the accelerometer
- synchronisation of the accelerometer and the imager sensors

Furthermore, compression implies undersampling, so that even if the tool speed is calculated accurately, recovery of the image may be imperfect.

Image orientation/Tool rotation. As the logging cable is wound around its drum, it is twisted round its axis. This in turn causes the tool to rotate as the twist unwinds. The rotation is usually quite slow. Fast rotation occurs when the tool is prevented from rotating, for example by pad friction, so that a large torque builds up before finally, the tool is free to rotate. Fast rotation also occurs frequently at the start of a log, when during the downward trip, the tool touches the bottom and stops rotating before all the twist in the cable has been completely unwound.

Inclinometry data acquired with an imager tool allow the image to be correctly oriented, even when the tool rotates. One rotation every ten metres, is often quoted as the limit above which inclinometry measurements and dip computations would begin to lose accuracy. Modern instrumentation can in fact cope with rotation rates up to one rotation every two metres. Correctly oriented images have been obtained for up to one rotation per metre. It is possible that some dip computation programs, based on

button correlation methods, may run into difficulty if the tool rotates significantly (e.g. $>90°$) within the length of the correlation window, which is usually of the order one metre. Dips picked interactively on a workstation would be unaffected by rotation, as long as the image itself is correctly oriented.

It must be pointed out that *apparent* excessive rotation can be caused by (a) incorrect speed correction, when a log is compressed/stretched erroneously, and (b) when the inclinometry measurements are in error. Apart from outright failure of the instruments, magnetometer measurements are notably prone to error in the proximity of casing. These possibilities should always be investigated if the image orientation appears to be abnormal. In the early days of horizontal wells, images were often oriented incorrectly, using 'North' as the reference, i.e. orienting the image such that 'North' is the left edge of the image. In horizontal wells, the definition of 'North' in the plane perpendicular to the tool axis can be ambiguous, and the top-of-hole direction should be used as reference instead.

Signal strength (applied voltage and gain). During acquisition, the voltage applied between the pad and the current return may be adjusted using a feedback loop, so as to obtain a button current level above noise, and below saturation for the electronics. In addition, on some tools, a gain can be applied to low signal levels before digitization, so as to avoid the introduction of quantization noise. Despite these mechanisms, in adverse conditions, such as when the ratio of formation resistivity to mud resistivity is very high, the signal level will be low and affected/dominated by noise. In such cases, the image will have a speckled aspect as illustrated by L&B 'Extremes of condition'.

If a variable voltage and/or gain have been applied, the measured currents must be corrected in order that they reflect the formation conductivity. Such a correction is usually taken care of automatically in the processing. If the correction is omitted by mistake, or if it is impossible to make the correction because the voltage and gains data are lost, anomalies in image intensity will occur. Without the corrections, the contrast between different beds will be reduced or even reversed for widely separated beds. However, these errors are not often easy to notice. A much clearer indication of this omission is a mismatch in intensity between the images from pads/flaps in the neighbourhood of a boundary of sharp contrast, where a gain or voltage change has taken place. Because the gains and voltages are applied as functions of time, images from pads/flaps which are offset in depth will show the effects of the gains and voltage changes at different depths (equal to the depth offset), leading to an intensity mismatch which is easily recognizable.

Button equalization, faulty buttons. The response of individual buttons are seldom identical because of limitations in manufacturing, and/or accidental factors during logging. Among the latter are uneven pad contact, mechanical wear, and deposition of mud/oil on the pad face. These lead to stripes in the image when buttons on the same pad have a markedly different response, or unevenness in the intensity of the different pads. In addition, certain buttons may fail to work at all, when the electronics fail. Such failures may be permanent or intermittent. e.g. L&B 'Button or Flap Death'.

To remove this unequal response and to detect faulty buttons, the following post-acquisition processing may be carried out. The mean and variance of the buttons are computed over a long window ($\approx$5 m). If the mean and variance for a given button are close enough to the median values for all buttons, then the button response is 'equalized' by a 'gain and offset' operation, such that mean and variance become equal to their respective median values without disturbing the detailed variations. Buttons which are defective are detected as having abnormal mean and variance values. Values of faulty buttons occurring in isolation are replaced by interpolation using values from adjacent working buttons. Equalization works if it can be assumed that over an interval of $\approx$5 m all buttons functioning normally would have the same average response.

L&B 'Drilling induced breakout' shows an interval where the images from different pads are not correctly equalized. In this interval, the buttons evidently do not have the same average response, since the pads are affected differently by the breakout. So the equalization correction breaks down.

Striping (mud smear) problems are observed in L&B 'Mud smears', L&B 'Drilling Induced Fractures' and L&B 'Spiral Hole'. Either the equalization correction has not been applied, or it has broken down because the buttons are affected differently by fractures, or irregular contact in the spiral hole.

L&B 'Faulty button correction' is an example where a circuit failure has caused every third button to fail. (In the tool concerned, the data from every third button is processed by the same electronic circuit.) This in turn causes the speed correction using button correlations to work incorrectly. The result is vertical striping

throughout the image (faulty buttons uncorrected), and discontinuous bedding features and 'saw-teeth' (incorrect speed correction) in the left hand image. In the corrected right hand image, the faulty buttons are correctly detected and excluded from the speed correction calculation. The image is therefore improved in two ways: by a better speed correction and by the replacement of faulty button values by interpolation.

Distortion by strong contrast. Currents tend to follow a path of minimum resistance, directing themselves towards conductive regions and away from resistive ones. When imaging small objects such as vugs and nodules, the conductive ones will appear larger, as currents from nearby buttons are drawn towards them (i.e. the object is 'seen' by more buttons than it should), while resistive ones appear smaller. Similarly, conductive beds will appear thicker while resistive ones appear thinner (Trouiller *et al.* 1989). These distortions are proportional to the conductivity contrast across the object boundary. When the contrast is high, halo effects are observed, as shown in L&B 'Halo effects conductive/resistive' and 'Fracture aureoles'. These observed effects are confirmed by modelling (Trouiller, *pers. com.* 1989) and a simple explanation based on the modelling results is given below.

The response of the button current to inhomogeneities is most readily understood in terms of current lines which indicate the *direction* followed by a current originating from a point on the pad surface. Figures 3a–d show the current lines (shown as arrows) emerging from the pad face and entering the formation in front of four different conductivity inhomogeneities:

(a) conductive nodule
(b) resistive nodule
(c) dipping resistive plane or fracture
(d) dipping conductive plane or fracture

The diagrams are schematics and do not correspond to precise computations. The areas shown correspond to the first few centimetres of formation facing the pad. The resistivity contrast between the conductive areas (dark), and resistive one (light) would be about 1:100.

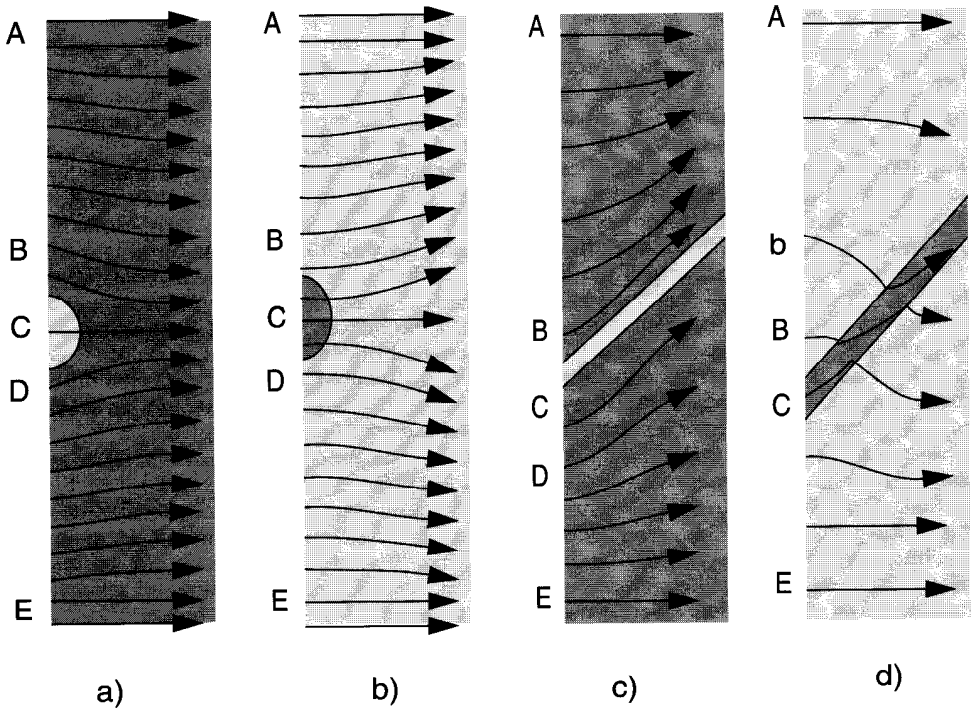

Fig. 3. Schematic showing current lines emerging from the pad face of an microresistivity device (left side of diagram) into the formation in the neighbourhood of: (**a**) a small resistive nodule, (**b**) a small conductive nodule or vug, (**c**) a thin resistive bed or fracture, and (**d**) a thin conductive bed or fracture. The shading of the formation is light for resistive and dark for conductive.

As the conductive pad face is an equipotential surface, the current lines are initially perpendicular to the pad. Subsequently, the lines are directed in space according to the following 'tendencies':

- aligned perpendicular to the surface of conductive bodies, since these tend to be equipotential surfaces
- aligned parallel to the surface of highly resistive bodies, since the current tries to avoid such regions
- avoid each other since current lines cannot intersect

The current emerging from a button will follow a path prescribed by a tube containing all the current lines originating from the button surface. For a given potential applied between the pad and the return electrode, the current will be proportional to the conductance of the path. The conductance of a given length of path will be proportional to the product of the conductivity of the formation along the path, and the cross-sectional area of the tube of current lines. Referring to the diagrams, we can say that the button current will be relatively strong if firstly the current lines pass through a conductive part of the formation, and secondly if the current lines are divergent, indicating a large cross-sectional area. Conversely, the current will be relatively weak if the path passes through a resistive region or if the current lines are squeezed together.

In Fig. 3a, if a button was placed at position A or E far away from the resistive nodule, the homogeneous background formation will read a normal current: the tube of current lines emerging from such a button will be entirely in the background formation, and the cross-sectional area of the tube will be 'average' since the current lines are neither divergent nor convergent. At position C facing the nodule, the current is low because the path passes through the resistivity nodule. These positions correspond to the bright zone in L&B 'Halo effects – resistive'. At positions B and D immediately on either side of the nodule, the current lines are entirely in the background formation, but spread out round the back of the nodule, implying an increased cross-sectional area. The current is therefore higher than average. At these positions, we observe the apparent conductive (dark) rim surrounding the resistive nodule.

In Fig. 3b, buttons at positions A or E far away from the conductive nodule, will again read a normal current for the homogeneous background formation. At position C facing the nodule, the conductance along the current path is high: firstly because the tubes of current lines pass through the conductive nodule, and secondly, because the current lines are divergent. Thus the current for a button at C will be high, corresponding to the black areas in L&B 'Halo effects – conductive'. At positions B and D immediately on either side of the nodule, the current lines are entirely in the background formation, but they are squeezed together, implying a decreased cross-sectional area. The current is therefore lower than average. At these positions, we observe the apparent resistive (bright) halo surrounding the conductive nodule.

Figure 3c represents the case of a dipping resistive bed or fracture, at the up-dip azimuth. The current lines are squeezed together at position B, so the button current at B will be lower than that at A. By contrast, at position D the current lines spread out, so the button current from D will read higher than that at A. This is observed in L&B 'Proximity effects – Fracture aureoles'. Above the crest of the fracture sinusoid, the image is white (low current) and below the crest, it is black (high current). Turning Fig. 3c upside down gives the situation at the down-dip azimuth. Below the lowest point of the sinusoid, the image is white (low current) and above it, the image is black (high current). L&B 'Cement mottling' is a more complicated example of the same effect.

Figure 3d, which represents the case of a dipping conductive bed or fracture in the up-dip azimuth, illustrates the increased depth of investigation mentioned earlier. High currents will be registered by a button placed at C facing the conductive layer, but also at B and to a lesser extent b where the current path is drawn into the conductive layer deeper into the formation. In other words, at B and b the depth of investigation of the button is increased. On the image, the apparent position of the conductive feature will therefore be above C. Again, Fig. 3d can be turned upside down to see that the apparent position of the conductive bed will be below its true position in the down-dip azimuth. If a dip is computed from the button response, the dip magnitude will be too high. Note that unlike the three earlier cases, there are no obvious anomalies in the image to indicate that the tool response is distorted.

In general, it is difficult to correct for these geometrical distortions because the resistivities and geometry of the heterogeneities are unknown. Even if these are known, the only way forward would be extensive modelling which is impractical on a routine basis. The interpreter should be cautious when using images to obtain

bedding thickness, sand count, and dips, in the presence of strong resistivity contrasts.

In L&B 'Proximity features', dark patchy features are interpreted as 'Benthic shells in a mudstone' close to but not intersecting the borehole wall. While it is possible for heterogeneities with strong contrast situated away from the borehole wall to be observed in a microresistivity image, it would be difficult in general to distinguish them from weakly contrasted ones exposed on the borehole wall. The fact that microresistivity devices have a finite depth of investigation can pose ambiguities in the interpretation.

Standoff/mudcake. Since the resistivity contrast between mud and mudcake is small, mudcake and standoff have similar effects on microresistivity devices. If there is standoff between pad and formation, due to mudcake, rugosity, washouts, breakouts, drilling damage or well deviation, the focusing effect of the pad face in the formation will diminish, leading to a loss in resolution initially, and eventually, to total loss of the image. Generally speaking, small standoffs (<5 mm) are barely noticeable while standoffs greater than 2 cm will render an image too blurred to be of value. In addition, opposite a large standoff, the button responds to the mud conductivity.

L&B 'Spiral Hole', 'Drilling induced breakout', 'Rugose Hole' and 'Mudcake Buildup' are examples where standoffs have caused blurring or loss of parts of the image. The caliper logs should be used for confirmation if standoff appears to be a problem. Again, standoff effects cannot be corrected in practice.

Ultrasonic imagers

Tool operation

The borehole televiewer tool was invented by Zemanek *et al.* (1969). Modern versions commercially available include the CBIL (Faraguna *et al.* 1989), CAST (Seiler *et al.* 1990) and UBI (Hayman *et al.* 1994). The above references give a detailed description of the characteristics of these tools.

Ultrasonic tools work on the pulse-echo principle. Ultrasonic pulses at a frequency between 250 kHz and 500 kHz are emitted from a rotating transducer towards the formation, at up to about 250 times per revolution. The same transducer captures the reflected pulses, from each of which an amplitude and a transit time are extracted and recorded. An image of the borehole wall can be reconstructed with either the amplitude or transit time data. To make an image, the logging speed must match the rotation speed of the transducer i.e. one rotational scan is made per vertical sampling interval. Focused transducers are used in modern tools to improve signal strength and decrease sensitivity to rugosity.

The commercial tools differ in the way the transit time and amplitude are measured. Some use the method of the original televiewer. The transit time is measured as the time when the signal first exceeds a threshold, in a time window where the reflected signal is expected to arrive. The amplitude is measured as the largest amplitude value measured in the window. The transit time and amplitude so measured correspond to the same arrival if the first arrival is the strongest. This is most often but not always the case. In later tools, the reflected waveform in the window is digitized. The amplitude and transit time are then obtained by digital processing methods. For example, the waveform envelope is computed to obtain the amplitude and transit time corresponding to its peak. In either case, the detection window moveout is regulated by a feedback loop based on the previous detection.

Tool response

Transit time measurement. The transit time gives the distance between the transducer and the borehole wall once the mud velocity is known. The mud velocity is often logged by the ultrasonic imager, so that the transit time image is transformed into an image of the borehole radius. The radius image is above all a survey of the hole shape and is the preferred method to study breakouts (Barton *et al.* 1997). Bed boundaries, fractures and small homogeneities will be visible in the transit time/radius image if they cause the borehole radius to change. Sand and shale beds are often distinguishable on the radius image because of differences in the borehole radius (Hayman *et al.* 1994). Only large fractures and vugs are normally visible on the transit time image.

Amplitude measurement. Considerably more details are observed on the amplitude image than the radius image. The amplitude is influenced by the following factors:

- surface roughness/continuity
- acoustic impedance contrast between mud/mudcake and formation

- angle of incidence
- length of path traversed and attenuation in mud

The first effect is usually the most important from the interpretation point of view, allowing fractures, vugs, beds and other inhomogeneities to be observed. Changes in acoustic impedance contrast allows beds to be distinguished, if a sufficiently large acoustic impedance contrast exists. The last two effects do not convey any information which is not already in the radius image. One of the aims of processing is normally to remove these latter two effects.

Depth of investigation and resolution. The depth of investigation of a reflection measurement is effectively zero. The beam width is maintained at ≈4 mm at 500 kHz and ≈8 mm at 250 kHz for different hole sizes by using transducers with either different focal lengths or mounted with a different radial offset. The beam width doubles for a given transducer if the transducer-reflector distance is increased to about 5 cm above the nominal hole radius. While beam size controls resolution, objects smaller than beam size can be detected.

Although the theoretical resolution of ultrasonic imagers is similar to that of a microresistivity imager, comparison of the two types of images shows that more small features are visible in the latter. This is because the range of resistivity values occurring in rocks (two or three decades) is much larger than the range of acoustic impedance values (less than a decade).

Response to fractures. Schmidt *et al.* (1992) give a detailed account of the pulse-echo response to fractures. This shows that apertures below 0.1 mm can be detected. Like the microresistivity measurement, the integrated amplitude response can be related to fracture aperture. However, since the amplitude is also sensitive to the roughness at the intersection of the fracture with the borehole wall, this method gives only a rough indication of aperture.

Comparison with microresistivity images show that the ultrasonic devices detect only the larger, open fractures. This should not necessarily be viewed as a disadvantage, especially when both types of devices are used in synergy.

Special features related to artefacts

Speed correction. Ultrasonic images can be subject to irregular logging speed, much as other logs (L&B 'Tool Speed Irregularities – Stuck zones, Stick zones'). This results in stretching and compressing of the image as explained earlier. Unlike the microresistivity imagers, the image is not derived from interlacing sensors which are offset in depth, so there are no 'saw-teeth' mismatches. In one sense this is a benefit while in another sense, it is a disadvantage: (1) just because saw-teeth artefacts cannot occur does not mean that image compression has not occurred, and, (2) the off-depth microresistivity sensors do allow an 'image-based' speed correction to be applied.

A problem relating to tool speed is the requirement that the rate of rotation of the transducer matches the vertical sampling. If the tool is rotating too fast or too slow relative to the logging speed, periodically, there will be a surplus or deficit of one scan. The surplus is usually discarded and the deficit made up by repeating a previous scan. In either case, there will be a discontinuity in the image. If this occurs frequently, the image will have a 'blocky' character. This requirement means that the logging speed for ultrasonic imagers is two or three times lower than that for microresistivity imagers. Experience shows that low logging speed often results in an increase in tool speed variations.

Tool eccentering. Eccentering causes the amplitude to increase at those azimuths where the tool is closer to the borehole wall and vice versa. Small to moderate eccentering (<1 cm say) induces a variation in signal strength which may obscure finer details on the borehole wall (L&B 'Eccentralisation/Standoff'). This is essentially a display problem: when changes in radius dominate the changes in amplitude, the smaller amplitude variations due to fine details translate into one or two adjacent colours on the colour scale, and become difficult to visualize. Data are not lost. On the other hand, with severe eccentering, the signal may be lost altogether from certain azimuths where the reflected pulse no longer returns to the transducer.

Provided there is only a small loss of data, the effects of eccentering can be readily removed. From the radius data, the actual location of the tool centre relative to the borehole centre can be determined by solving a relatively simple geometrical problem, and the effects of eccentering on the radii values can be corrected. To correct the amplitude, Menger (1994) describes a method using the known tool position in the borehole and known characteristics of the tool. However, this method requires that the tool is calibrated uphole in a fluid similar to the mud used. More generally, a variety of image filters can be applied to remove the most obvious

effects of eccentering. For example, the effects of eccentering in the form of the first and second harmonic variation of the amplitude can be removed by a suitably designed filter.

Irregular hole shape. Irregular hole shapes such as washouts (L&B 'Washout') and spiral holes caused by drilling (L&B 'Tool Orbiting', L&B 'Spiral Hole') pose serious problems for the ultrasonic scanners. Hole shape irregularities produce very much the same effects as eccentering, except that the changes in signal are much less gradual and less predictable. When there is severe signal loss, then as with severe eccentering, there is nothing to be done. When signal loss is limited, the eccentering correction can help to improve the image in some cases.

Certain deformations on the borehole wall caused by the drilling process give rise to 'vertical stripes' e.g. L&B 'Keyseat Furrow', L&B 'Stabilizer grooving'. These effects can often be diminished using image filters, or by 'equalizing' the image along vertical stripes as described under 'Button Equalization' for microresistivity imagers.

Signal loss. As mentioned earlier in connection with eccentering and irregular hole shape, signal loss can result when the reflected pulse fails to return to the transducer, due to large angles of incidence. In addition, signal loss can also result from attenuation of the signal in heavy muds, or when a sudden increase in travel time, due to an abrupt change in hole shape, causes the return pulse to fall outside the detection time window.

Signal loss is usually indicated by white spots on an ultrasonic image. L&B 'Signal Loss' shows an example of signal loss due to an irregular/enlarged hole.

Mudcake. Information concerning *in situ* mudcake properties is difficult to come by, so it is impossible to be quantitative concerning details of the interaction between the ultrasonic pulse and the mudcake. Qualitatively, mudcake *in situ* should behave much like mud, except that the velocity and attenuation of sound are both increased. The acoustic contrast between mud and mudcake is weak as compared to that between mudcake and formation, so the pulse is effectively reflected at the formation surface. Thus the presence of mudcake usually causes a drop in amplitude and a decrease in transit time. Normally, it would be difficult to detect mudcake since many lithology changes are also associated with the same changes. However, since the mudcake is fragile, the passage of centraliser/stabilizer arms will remove some mudcake along their tracks. This gives rise to artefacts on the ultrasonic images (amplitude and radius) which are difficult to mistake. See L&B 'Stabilizer grooving', 'Noise: 60 Hertz' and 'Mudcake Build-up'. (Note that the tracks of the arms are not strictly vertical, but should be parallel to a curve such as relative bearing (RB), giving tool rotation.)

In all the three examples cited above, it is evident that bedding features can be observed even in the presence of mudcake. It is unclear if these are observable because the change of lithology has led to changes in reflectivity and rugosity at the formation surface, or to the thickness and consistency of the mudcake itself.

60 Hz noise. L&B '60 Hz Noise' shows an artefact which is particular to the UBI tool. It appears only on the amplitude image.

If the 60 Hz variation of the power supply is not effectively screened out, the pulse emitted by the transducer, and hence the received amplitude, will be modulated by a 60 Hz variation. Since the transducer rotates about seven times a second, and the rotation is coherent with the 60 Hz voltage variation, there will be eight periods of image amplitude variations per rotation, with a small phase shift between rotations, resulting in the observed eight-fold spiral or diagonal stripes. The 60 Hz noise can be readily removed by a filter.

Wood grain pattern. The L&B 'Wood Grain' examples for the UBI and CBIL tools have quite unrelated causes. As reported in L&B, the patterns for the CBIL/STAR tool are caused by interference of reflections associated with the housing surrounding the transducer. The pattern for the UBI is caused by a bias in the interpolation algorithm. The artefact appears on both the amplitude and the radius images of the UBI, with an exact correspondence between the patterns. An explanation for this bias effect is as follows.

During acquisition, the reflected waveform is sampled by the UBI at discrete time intervals and digitized. The transit time is obtained as the time corresponding to the peak in the waveform envelope. At the first instance, the transit time obtained would be an exact multiple of the sampling interval Δ. An interpolation formula is then applied to obtain more accurate values of the peak location and amplitude. This yields a transit time which can be expressed as an exact multiple of Δ plus a fractional part. The three-point interpolation formula used introduces a bias if the waveform envelope near the peak is non-parabolic.

Figure 4 shows the values of transit time in a small part of a scan. The continuous curve shows the slowly varying transit time values that the tool should have measured. The dashed line shows the discretized values $(n-1)\Delta$, $n\Delta$, $(n+1)\Delta$ measured before interpolation. The dotted lines and arrows show the sampled values obtained by interpolation. The interpolated values are observed to show a preponderance of fractional values centred at say 0.5Δ. This gives rise directly to the wood grain pattern in the transit time (or radius) image; contour lines are compressed at values close to integer values of Δ, and spaced out whenever the fractional values are $\approx 0.5\Delta$.

Note that the wood grain is observable only when the transit time changes by amounts much smaller than Δ between many successive samples. Δ is a small quantity (0.1 μs) which corresponds typically to a radius change of <0.08 mm in water. So the borehole must be smooth and the tool well centred to observe the bias effect. A corresponding pattern appears on the amplitude image also, since the amplitude varies approximately linearly with transit time when the transit time varies within close limits.

The bias can be removed only on a statistical basis since it depends on the shape of the waveform envelope, which is variable. If we take many transit times measured over a large depth interval, then the fractional part should be uniformly distributed between zero and one since all fractional values are equally likely to occur. If however, the pattern shown in Fig. 4 is repeated systematically, then a histogram of counts versus fractional values would have a peak centred at ≈ 0.5. From such a histogram, one can derive a correction to the fractional part of the transit time that will yield a uniform distribution, and hence remove the wood grain pattern from the transit time image. From a crossplot of amplitude and transit time, the amplitude can be modified in parallel with the transit time, and the wood grain in the amplitude image is reduced. Since the processing for the amplitude involves this additional correlation, removal of the wood grain pattern is less effective.

Gain calibration. In the UBI tool, a variable gain is applied to the emitted pulse according to the strength of the previously received signal. Since the received amplitude is divided by the gain before recording, the amplitude is nominally corrected for the applied gain. However, the gain applied electronically may not lead to a proportional gain in acoustic amplitude. It is therefore necessary to calibrate the gains, and recorrect the amplitudes. If the gains are not calibrated, the image will appear spotty as shown

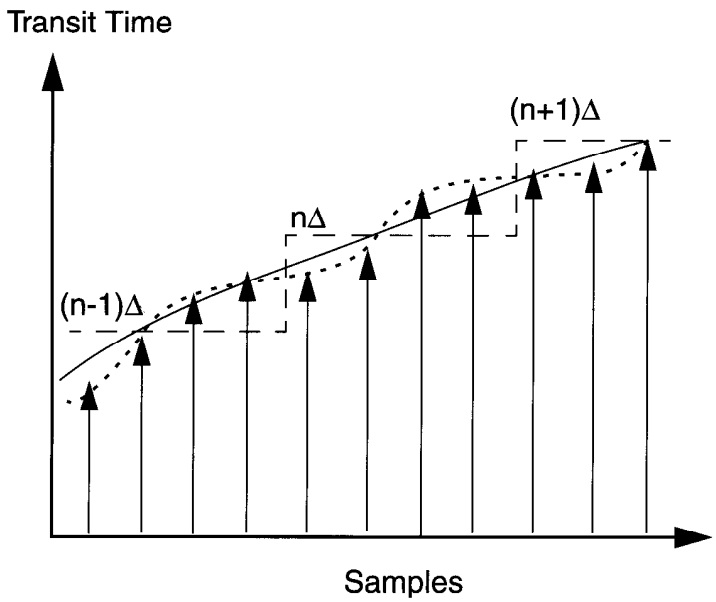

Fig. 4. Schematic showing how wood grain patterns arise as a result of bias in the interpolation of transit times. The full line shows the values that should have been measured. The dashed line shows the discretized values measured before interpolation. The dotted line and arrows show the values after interpolation.

in the L&B 'Honey-comb' example. This artefact is found only on the amplitude image of the UBI.

The calibration is done statistically. The gain applied may take one of 16 levels according to the strength of the previously received signal. To allow the calibration to work, this level is then *randomly* increased or decreased by one level. Now, if we take from the entire image, a large number of pairs of successive amplitudes (nominally corrected) where the gain has changed from level n to $n+1$, and compute the ratio of these pairs of amplitudes, we would expect the average value to be one. If the measured ratio is in fact $1:x$, then the gain of levels n and $n+1$ must be modified in the ratio $x:1$.

Discussion and summary

In this paper, the essential aspects of tool operation and processing of microresistivity and ultrasonic imaging tools have been described with reference to the artefacts described by Lofts & Bourke. From the measurement point of view, many features which are actually on the borehole wall are non-artefacts, and these have been excluded from the discussion. It is perhaps worthwhile pointing out that breakouts and induced fractures which are classed as artefacts in the sense of Lofts & Bourke, provide important data for the study of in-situ stress and well stability (Barton *et al.* 1997). Similarly, marks left by packers, sidewall core samplers, fluids samplers etc. provide important information when analysing the corresponding test/data. Mud smears and mudcake effects also make a positive contribution to interpretation, by indicating or confirming oil-bearing and permeable zones respectively.

An understanding of the similarities and differences between the microresistivity and ultrasonic images is important in the choice of tool for a given environment, and can be helpful even when interpreting the images separately. Some of the more important points concerning the use and interpretation of the two types of images are summarized below. It is noted that the two types of images are complimentary. Hayman *et al.* (1994) and Hansen & Parkinson (1999) show how interpretation can indeed be enhanced when both types of images are available.

Tool response. Microresistivity devices appear to 'see more'. This is mainly because many lithologies and geological features such as fractures, are more readily distinguishable on the basis of resistivity contrast as opposed to acoustic impedance contrast and other properties on which the ultrasonic response depends. The slightly higher resolution of the microresistivity devices also contribute by making small heterogeneities and thin beds distinct.

Microresistivity buttons have a finite but variable depth of investigation, and the response is distorted in the presence of strong resistivity contrast. These effects can give rise to ambiguities concerning dip values and the exact location of small features in certain cases. Ultrasonic devices respond only to features which are on the surface of the borehole wall so there is no ambiguity concerning their location.

Microresistivity imagers see large as well as relatively small fractures, whether they are open or in-filled with conductive or resistive material. Moreover, if the in-filling material is conductive, and its conductivity known, an estimate can be made of the aperture, even for values much below tool resolution. Ultrasonic imagers see mainly large, open fractures. There are no reliable methods to estimate aperture.

As the microresistivity physics is somewhat complex, it is worthwhile mentioning that mathematical modelling is indispensable for clarifying the underlying causes of anomalies observed.

Hole condition. Both tool types are affected by irregular hole shape, but especially the ultrasonic tool. Spiral holes associated with turbo-drilling appear to be a particularly serious problem. Since bad holes are also the underlying cause of speed correction problems, a good borehole is a crucial factor for good images.

Mud, mudcake. Microresistivity devices only work in conductive mud. Ultrasonic imagers work in all types of mud in principle, provided attenuation is not too severe. The presence of mudcake is an important indication of permeability. We mentioned earlier how the ultrasonic imager provides a robust way to detect mudcake. Microresistivity imagers are insensitive to mudcake by comparison.

Hole size and coverage. Microresistivity tools will operate in hole diameters up to about 40 cm, which correspond to the maximum opening of the arms. Coverage of the borehole wall, which is never 100% except in very small holes, will decrease linearly with hole size. For a hole diameter of 20 cm, the coverage is typically 10% per pad (i.e. 80% for a eight-pad tool, 60% for a six-pad tool). Resolution will be unchanged with hole size for the same pad contact conditions.

Ultrasonic tools gives 100% coverage, unless signal is lost due to very large tool eccentering.

The maximum hole size for ultrasonic imagers is limited by the attenuation of sound in the mud, and the focal point of the transducer. In a light mud, the maximum hole diameter would be about 30 cm. At the largest hole sizes, there is a decrease of resolution, due to defocusing, signal attenuation and increase in the lateral distance between samples on the borehole wall.

Conclusion

In this paper, the essential aspects of tool operation and processing of microresistivity and ultrasonic imaging tools are described. A particular reference has been made to the artefacts described by Lofts & Bourke, with the intention of giving a fuller explanation of the origins of the anomalies, and indicating whether the distortions can be remedied by processing. With the few exceptions stated explicitly, the discussion should be valid for all the commercially available tools since they operate in a similar way.

The author thanks the two referees for many useful suggestions, and J.-C. Trouiller for his help to clarify various issues concerning the microresistivity tool.

References

BARTON, C. A., MOOS, D., PESKA, P. & ZOBACK, M. D. 1997. Utilizing wellbore image data to determine the complete stress tensor: application to permeability anisotropy and wellbore stability. *The Log Analyst*, **38**(6), 21–33.

BOURKE, L., DELFINER, P., TROUILLER, J.-C., FETT, T., GRACE, M., LUTHI, S. M., SERRA, O. & STANDEN, E. 1989. Using Formation MicroScanner images. *The Technical Review*, **37**(1), 16–40.

CHAN, D. S. K. 1984. Accurate depth determination in well logging. *IEEE Transactions on Acoustics, Speech and Signal Processing*, **32**(1), 42–48.

CHAPELLAT, H., BERARD, M. V. & CHEUNG, P. S. 1996. *Method and Apparatus for Determining a Depth Correction for a Logging Tool in a Well.* US Patent No. 5522260.

EKSTROM, M. P., DAHAN, C. A., CHEN, M. Y., LLOYD, P. M. & ROSSI, D. J. 1987, Formation imaging with microelectrical scanning arrays: *The Log Analyst*, **28**(3), 294–306.

FARAGUNA, J. K., CHACE, D. M. & SCHMIDT, M. G. 1989. An improved borehole televiewer system: image acquisition, analysis and integration. *Transactions of the 30th Annual Logging Symposium of the Society of Professional Well Log Analysts*, paper UU.

HAYMAN, A. J., PARENT, P., CHEUNG, P. S. & VERGES, P. 1998. *Society of Petroleum Engineers Production and Facilities*, **13**, 5–13.

HANSEN, T. & PARKINSON, D. N. 1999. Insights from simultaneous acoustic and resistivity imaging: *This volume.*

HORNBY, B. E., LUTHI, S. M. & PLUMB, R. A. 1992, Comparison of fracture apertures computed from electrical borehole scans and reflected Stoneley waves: an integrated interpretation. *The Log Analyst*, **33**(1), 50–66.

LACAZETTE, A. 1996. *The STAR (SimulTaneous Acoustic and Resistivity) Imager.* London Petrophysical Society (SPWLA Chapter) presented at the LPS Borehole Imaging Seminar.

LOFTS, J. C. & BOURKE, L. B. 1999. The recognition of artefact images from acoustic and resistivity devices: *This volume.*

LUTHI, S. M. & SOUHAITÉ, P. 1990. Fracture apertures from electrical borehole scans. *Geophysics*, **55**(7), 821–833.

MENGER, S. 1994. New Aspects of the Borehole Televiewer Decentralization Correction. *The Log Analyst*, **35**, 14–20.

SAFINYA, K., LE LAN, P., VILLEGAS, M. & CHEUNG, P. S. 1991. Improved formation imaging with extended micro-electrical arrays. *Society of Petroleum Engineers*, **SPE-22726**, presented at the 66th SPE Annual Technical Conference and Exhibition, Dallas, Texas 1991.

SCHMIDT, M. G., LI, X. STEINSIEK, R. R. & MA, T. A. 1992. Numerical model for predicting ultrasonic transducer pulse-echo response to borehole fractures. *Transactions of the 33rd Annual Logging Symposium of the Society of Professional Well Log Analysts*, paper **U**.

SEILER, D., EDMISTON, C., TORRES, D. & GOETZ, J. 1990. Field performance of a new borehole televiewer tool and associated image processing techniques. *Transactions of the 31st Annual Logging Symposium of the Society of Professional Well Log Analysts*, paper **H**.

——, KING, G. & EUBANKS, D. 1994. Field test results of a six-arm microresistivity borehole imaging tool. *Transactions of the 35th Annual Logging Symposium of the Society of Professional Well Log Analysts*, paper **W**.

TROUILLER, J-C., DELHOMME, J-P., CARLIN, S. & ANXIONNAZ, H. 1989. *Thin-bed reservoir analysis from borehole electrical images. Society of Petroleum Engineers*, **SPE-19578**, presented at the 64th SPE Annual Technical Conference and Exhibition, San Antonio, Texas 1989.

ZEMANEK, J., GLENN, E. E., HOLCOMB, S. V., NORTON, L. J. & STRAUS, A. J. D. 1969. The borehole televiewer – A new logging concept for fracture location and other types of borehole inspection: *Journal of Petroleum Technology*, **21**, 762–774.

WILLIAMS, C. G., JACKSON, P. D., LOVELL, M. A. & HARVEY, P. K. 1997. Assessment and interpretation of electrical borehole images using numerical simulations: *The Log Analyst*, **38**(6), 34–43.